Thermal and Mechanical Properties of a Polypropylene Nanocomposite

Thomas S. Ellis, Joseph S. D'Angelo

Delphi Research Labs, 51786 Shelby Parkway, Shelby Township, Michigan 48315

Received 23 October 2002; accepted 3 February 2003

ABSTRACT: An experimental polypropylene (PP) nanocomposite, containing approximately 4 wt % of an organophilic montmorillonite clay, was prepared and characterized, and its properties were compared with those of talc-filled (20–40 wt %) compositions. Weight reduction, with maintained or even improved flexural and tensile moduli, especially at temperatures up to 70°C, was a major driving force behind this work. By a comparison with the analytical data from a nylon 6 (PA-6) nanocomposite, it was found that the PP nanocomposite contained well-dispersed, intercalated clay particles; however, X-ray diffraction, transmission electron microscopy, dynamic mechanical analysis, and permeability measurements confirmed that exfoliation of the clay in PP was largely absent. The increased glass-transition temperature (T_g) of a PA-6 nanocomposite, which possessed fully exfoliated particles, indicated the molecular character of the matrix–particle interaction, whereas the PP nanocomposite exhibited simple matrix–filler interactions with no increase in T_g. The PP nanocomposite exhibited a weight reduction of approximately 12% in comparison with the 20% talc-filled PP, while maintaining comparable stiffness. Undoubtedly, considerable advantages may be available if a fully exfoliated PP nanocomposite is fabricated; however, with the materials available, a combination of talc, or alternative reinforcements, and nanocomposite filler particles may provide optimum performance. J Appl Polym Sci 90: 1639–1647, 2003

Key words: poly(propylene) (PP); nanocomposites; density; mechanical properties

INTRODUCTION

An attractive feature of polymer nanocomposites is the promise of significantly improved stiffness and tensile strength for a minor increase in specific gravity (SG) over the unmodified polymer. The initial successes of polyamide nanocomposites[1] have attracted most of the developmental interest to date, but there is intense interest in formulating treated clays that are suitable for polyolefins.[2–10] The published information has also highlighted some of the technical difficulties in achieving this goal.[3] There are claims suggesting that polypropylene (PP) nanocomposites have been developed; however, most of the published data suggest that well-dispersed and intercalated clay-modified polyolefins have been made rather than the more desirable nanocomposites[11] with fully exfoliated clay particles.

Filled PP, containing 20–40 wt % talc, is used extensively because of a combination of stiffness, dimensional stability, and, importantly, low cost. A major interest of this investigation was an evaluation of a PP nanocomposite that was expected to exhibit significantly increased stiffness for a reduction of weight in comparison with talc-filled polypropylenes (TFPPs). Material density reduction is a powerful driver for the development of new materials, and PP-based nanocomposites, which contain only 3–6 wt % of a nanoscale (~1 nm thick) platy filler, offer a potential route to this goal. A PP nanocomposite would also retain all the inherent attractive features of a polyolefin, such as moisture resistance and ease of processability. The characterization of the exfoliated state in a polymer matrix remains a difficult and semiquantitative task. Accordingly, we have used nylon 6 (PA-6) nanocomposites as a reference material to compare the state of exfoliation of the nanocomposite in PP.

EXPERIMENTAL

Materials

The modified clay (I.31PS), a nanocomposite concentrate (C.31PS), and PP nanocomposite (I.31PS/PP) compositions were prepared by Nanocor, Inc. (USA). The treated clay was a free-flowing powder, with a mean particle size of 10–20 μm, derived from a montmorillonite clay treated with a silane coupling agent. The concentrate and PP nanocomposite were prepared with highly crystalline polypropylene (HCPP) supplied by Spartec-Polycom (Rochester, NY). The HCPP material was the same as that used to compound the talc-filled compositions.

The polymer/clay concentrate was a master batch containing 50–60 wt % treated clay, and the remain-

Correspondence to: T. S. Ellis (thomas.s.ellis@delphi.com).

Journal of Applied Polymer Science, Vol. 90, 1639–1647 (2003)

der was made up of maleic anhydride (MA)-modified PP and HCPP. The nanocomposite was melt-compounded at Nanocor by the master batch being put into pure HCPP with additional compatibilizer. The control samples used for comparison were Spartec-Polycom TFPPs (40% TFPP, 30% TFPP, and 20% TFPP) and HCPP.

The PA-6-based nanocomposites were obtained from Unitika, Ltd. (Japan). The material compositions are proprietary, but both are described as synthetic nanocomposites derived from an octadecylamine treatment, or a similar long-chain aliphatic amine treatment, of a synthetic mica. The M2350 material (2 wt % filler) is simply M1030 (4 wt % filler) melt-mixed with regular PA-6 (50:50).

Processing and rheology

The melt processing of all polymers was performed with a DSM Research miniextruder and mini-injection molder (The Netherlands). TFPPs, PP, and PP nanocomposites (I.31PS/PP) were processed for 1 min at 300 rpm at 185°C. The PP nanocomposite was also processed with a 5-min extended processing cycle at 185°C. Additional blends of PP and the PP nanocomposite concentrate (C.31PS) containing 90, 80, and 70 wt % HCPP were subjected to a 5-min, 300 rpm mixing cycle at 185°C. The sample size was approximately 3–4 g for each melt-compounding operation. The samples were molded as both tensile bar-shaped coupons (5 mm × 90 mm × 1.5 mm) and uniform slabs (12 mm × 60 mm × 2 mm). The mold temperature was 40°C.

Mechanical properties

Tensile testing was performed with an MTS 830 with a 225-kg (500-lb) load cell and a strain rate of 0.1 cm/cm/min with an initial gauge length of approximately 2.54 cm. Flexural testing was performed with an MTS 830 with a 22.5-kg (50-lb) load cell and a crosshead speed of 1.25 mm/min. A 2.54-cm span length was used on uniform coupons (12 mm × 60 mm × 2 mm). ASTM methods D 638 and D 790 were used for this study.

Analytical procedures

Differential scanning calorimetry (DSC) was performed with a PerkinElmer series 7 calorimeter at a heating rate of 10°C/min. The melting point is reported as the maximum of the melting endotherm. The heat of fusion was measured with respect to an indium standard. The samples were taken from coupons molded on a DSM miniextruder.

Dynamic mechanical thermal analysis (DMTA) was performed with a Polymer Laboratories DMTA Mk III over a temperature range of −70 to 130°C and at a heating rate of 1.5°C/min. Coupons (12 mm × 60 mm × 2 mm) were set up in a single-cantilever geometry and subjected to a frequency of 1 Hz.

Thermal mechanical analysis (TMA) was performed on samples for the determination of the coefficients of thermal expansion (CTEs) with a TA Instruments TMA 2940 (Wilmington, DE). The dimensional change was measured in the longitudinal (flow), crossflow, and thickness directions at a heating rate of 5°C/min. The samples were cut from the center of the coupons and ramped up to 75°C from −40°C. Each sample was run three times under the same temperature conditions and at the same rate, being cooled rapidly with liquid N_2 after each run.

Thermogravimetric analysis (TGA) was used to obtain correct weight percentages of talc and Nanocor clay in samples tested with a TA Instruments HI-Resolution TGA 2950. The samples, taken from molded coupons, were analyzed in the high-resolution mode and heated in air, up to 1000°C, at a rate of 50°C/min.

X-ray diffraction (XRD) was performed on molded samples with a Siemens D500 at a low angle. Transmission electron microscopy (TEM) analysis was performed with a Phillips 430T microscope operated at an accelerating voltage of 150 kV. TEM samples were obtained as 90-nm-thick microtomed sections.

SG was measured by Archimedean methods with methanol. Coupons were weighed dry and in a submerged state in methanol. The volume displaced by the slabs in methanol was calculated from the density of methanol (0.791 g/cm^3):

$$(W_d - W_m)/D_m = V \tag{1}$$

$$W_d/V = \mathrm{SG} \tag{2}$$

where W_d is the weight of a dry sample in air, W_m is the weight of a sample in methanol, D_m is the density of methanol, and V is the volume of a sample.

Permeability measurements, with toluene as the diffusing molecule, were performed on uniform coupons (12 mm × 60 mm × 2 mm) according to procedures described in the literature.[12] Coupons were weighed dry in air, and the average thickness (h) was determined. After full immersion in toluene at 25°C, the uptake was recorded gravimetrically as a function of time with a closed weighing bottle and a balance capable of measuring to an accuracy of 10^{-5} g. The samples were carefully dried with paper cloth before being weighed and were quickly placed back into toluene. An analysis of the data was performed in the same way as that described.[12] Therefore, by measuring the increase of mass (M_t) as a function of time t and plotting this as M_t/M_∞ versus $(t/h^2)^{1/2}$, we obtained a straight line of slope $4(D/\pi)^{1/2}$, from which

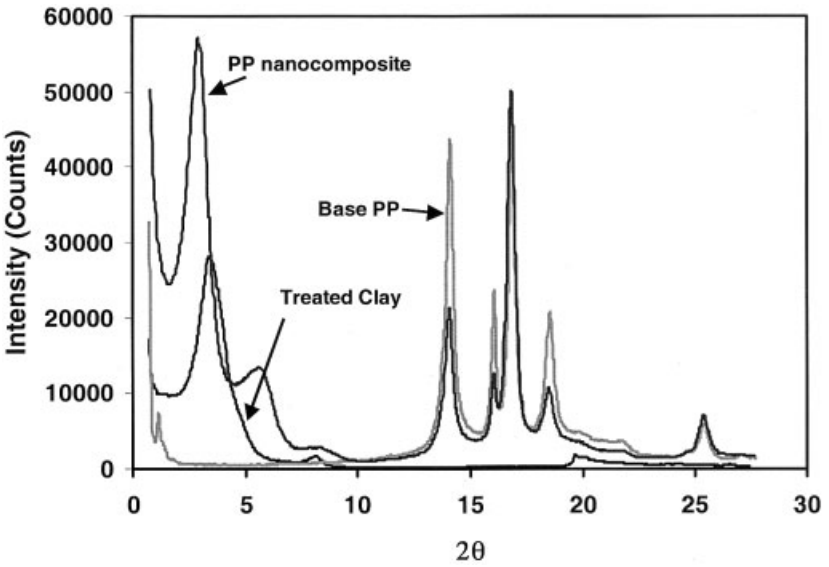

Figure 1 XRD patterns of the base PP resin, HCPP, treated clay (I.31PS), and PP nanocomposite (I.31PS/PP).

the diffusion coefficient (D) could be determined. The permeability coefficient (P) of a material is

$$P = DS \tag{3}$$

where S is the equilibrium solubility (g/g).

RESULTS AND DISCUSSION

Morphology and clay exfoliation

Previous studies[1–11] have already alluded to the utility of XRD and TEM for qualifying the degree of exfoliation of the clay in a polymer. For example, XRD is

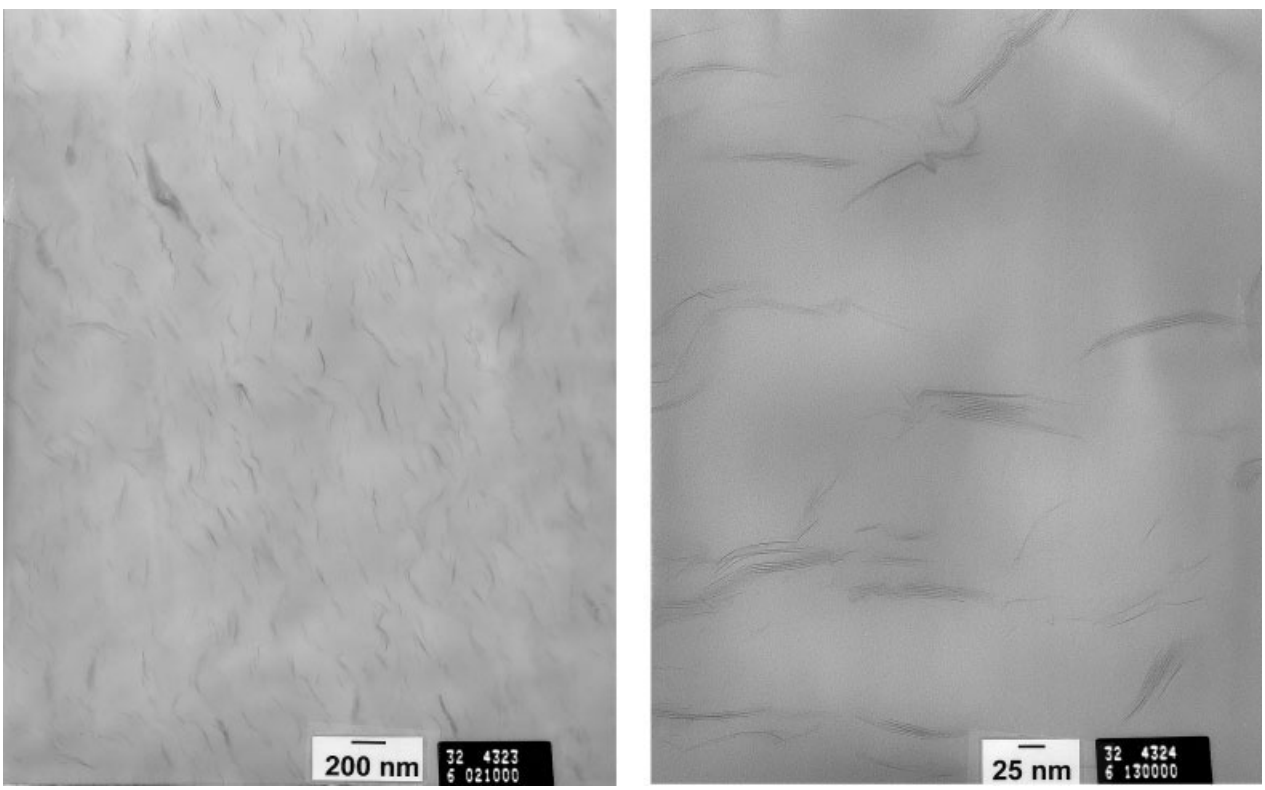

Figure 2 TEM micrographs of the PP nanocomposite (I.31PS/PP).

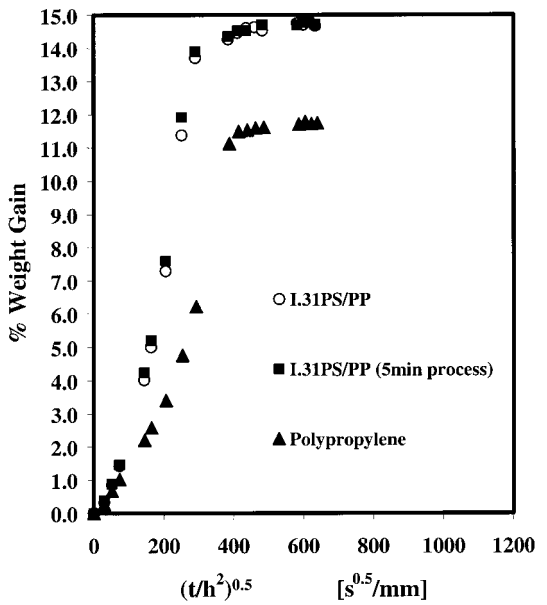

Figure 3 Uptake of toluene in PP and the PP nanocomposite (I.31PS/PP).

used to examine the intercalation and exfoliation of clay by monitoring the reflections from the silicate layers in the clay. The XRD pattern of the treated clay by itself, which obviously has no significant crystalline reflections from PP, is shown in Figure 1. It has a major reflection at approximately $2\theta = 3.5°$ associated with a *d*-spacing of 2.6 nm (26.1 Å). The XRD pattern of the clay in the PP nanocomposite, also shown in Figure 1, indicates a significant reflection at approximately $2\theta = 3°$, which corresponds to a *d*-spacing of 3.0 nm. A fully exfoliated nanocomposite would show no peaks in this region; however, an increased *d*-spacing indicates a wider separation of the silicate layers associated with polymer intercalation. The XRD patterns from the blends (10:90, 20:80, and 30:70) made from the concentrate and HCPP are similar to that of the PP nanocomposite, except that the peak associated with the clay progressively shifts to slightly smaller *d*-spacings. The latter signifies less efficient intercalation of PP into the galleries of the clay.

The crystalline reflections at approximately $2\theta = 14–19°$ originate from PP. The PP nanocomposite has a slightly different intensity of reflections than pure PP, and this indicates modification of the crystalline habit of PP in the PP nanocomposite. The differences do not appear as strong as that typically reported for PA-6. The main reflection at approximately $2\theta = 16°$, which is associated with the less ordered β-crystalline form,[13] appears to be reduced in the nanocomposite.

TEM micrographs shown in Figure 2 also support the inference of an intercalated PP nanocomposite rather than a fully exfoliated nanocomposite. The micrographs indicate a well-dispersed morphology with incomplete exfoliation. A sample subjected to extended melt processing for 5 min showed no differences. Although not shown here, the TEM micrographs that we obtained from the PA-6 nanocomposite showed a typical exfoliated structure similar to that reported in the literature.

Permeability of the polymer nanocomposites

Although evaluating the permeability of the composites was not a major objective of this study, measurements were performed to assist in their characterization. Additionally we have found that permeability can be an excellent indicator of intercalation versus exfoliation.

The foundation for the dramatically improved barrier performance of nanocomposites has been interpreted[14] mathematically, as shown by eq. (4). The major influence on permeability is caused by a significant reduction of *D*. For an impermeable filler of volume fraction ϕ_d, the composite permeability (P_C) is expressed in terms of a simple tortuosity factor (τ):

$$P_C/P_m = (1 - \phi_d)/\tau \tag{4}$$

$$\tau = 1 + (L/2W)\phi_d \tag{5}$$

where *L* and *W* denote the length and thickness of the platelets. For high aspect ratios, only a small quantity of filler causes a significant reduction in permeability. The equations describe a random orientation of particles so that any orientation of the platelets perpendicular to the transport direction would enhance barrier performance even further.

The measurements of the methanol permeability in the PA-6 M1030 (2.1×10^{-14} m^2 s^{-1}) nanocomposite indicate a greater than 10-fold reduction of permeability in comparison with that of an unmodified PA-6 (27.2×10^{-14} m^2 s^{-1}), clearly demonstrating the efficacy of exfoliation on reducing permeability. The re-

TABLE I
Measured Values of *D*, *S*, and *P* in Toluene at 25°C

	D (m^2 s^{-1})	S (g/g)	P (m^2 s^{-1})
Base PP (HCPP)	7.8×10^{-13}	0.117	9.1×10^{-14}
I.31PS/PP	3.1×10^{-12}	0.147	4.6×10^{-13}
I.31PS/PP (5-min extended process)	3.2×10^{-12}	0.147	4.8×10^{-13}

TABLE II
Summary of Material Thermal Properties

Material	% Ash	Melting point (°C)	Heat of fusion (J/g)	Crystallization exotherm maximum (°C)	Crystallization exotherm (J/g)
Base PP (HCPP)	0.098	164	101	123	98
I.31PS/PP	4.120	163	91	119	91
I.31PS/PP extended	—	163	91	120	92
20% TFPP	20.03	163	78	128	78
30% TFPP	—	165	68	131	70
40% TFPP	39.81	164	54	133	61

sults shown in Figure 3 and Table I clearly indicate an increased permeability to toluene in the PP nanocomposite in comparison with unmodified PP. This is almost certainly caused by the addition of the less crystalline MA–PP during melt compounding; however, the results support the conclusion of a well-dispersed, intercalated PP nanocomposite rather than a fully exfoliated composite. There was no difference observed between the nanocomposite processed with an extended mixing time and that processed under normal conditions. Evidently, increased time of shearing in the melt has little effect on the exfoliation of clay in PP.

The question of the miscibility of MA–PP with PP has not been addressed. If the MA content is relatively small, miscibility should be expected. This particular property may have a bearing on the exfoliation of the clay; however, in the absence of additional information, it remains an uncharacterized feature of the study.

Thermal properties

Table II summarizes the melting behavior, obtained by DSC, of some of the materials. Although the individual thermograms are not shown, all materials exhibited a single melting endotherm and a constant melting temperature (≈164°C). The degree of crystallinity of the polymer, as indicated by the heat of fusion, was also essentially constant once the mass balance of the polymer and filler was taken into account. Increased nucleation, caused by the filler particles, produced a shift to a higher temperature of the peak temperature of the crystallization exotherm on cooling from the melt.

TMA was applied to characterize the CTEs of the nanocomposite with respect to the HCPP and talc-filled materials. The results shown in Table III represent data as multiple scans of the same sample taken in three directions relative to the flow direction during molding. The recorded data were reasonably linear over the temperature range investigated. The CTEs were recorded from 0 to 60°C; for pure HCPP measured in the flow direction, the CTE was measured to be 1.19×10^{-4}/°C. The latter can be compared with a reference value (Moldflow database) of 0.944×10^{-4}/°C.

There are differences between the data from the various orientations; however, the highly talc-filled materials generally possess the lowest expansivity. The data indicate that the nanocomposite has properties comparable to those of 20 wt % TFPP, but the nanocomposite was found to have a slightly higher expansivity in the thickness direction. No study has been made to establish if the orientation of the clay platelets occurs to any significant extent. This would be expected to be a cause of anisotropic thermal expansion.

The PA-6 nanocomposite (M1030) has a literature CTE of 5.3×10^{-5}/°C; the CTE is 7–10×10^{-5}/°C for a general-purpose PA-6. The molding conditions and orientation may affect these values, but it is apparent that in a fully exfoliated state, the thermoplastic nanocomposite can exhibit a significant reduction in the CTE, and this suggests a strong filler-particle/matrix interaction.

The results from DMTA for PP nanocomposites fabricated by different routes are shown schematically in Figures 4 and 5. The peak in the loss modulus, associated with the glass-transition temperature (T_g), is

TABLE III
CTE (0–60°C)

	PP $\times 10^{-4}$ (°C)	I.31PS/PP $\times 10^{-4}$ (°C)	20% TFPP $\times 10^{-4}$ (°C)	30% TFPP $\times 10^{-4}$ (°C)	40% TFPP $\times 10^{-4}$ (°C)
Flow direction run 3	1.19	0.97	0.97	0.74	0.63
X-Flow direction run 3	1.31	1.24	1.18	0.96	0.87
Thickness run 3	1.31	1.53	1.45	1.42	1.23

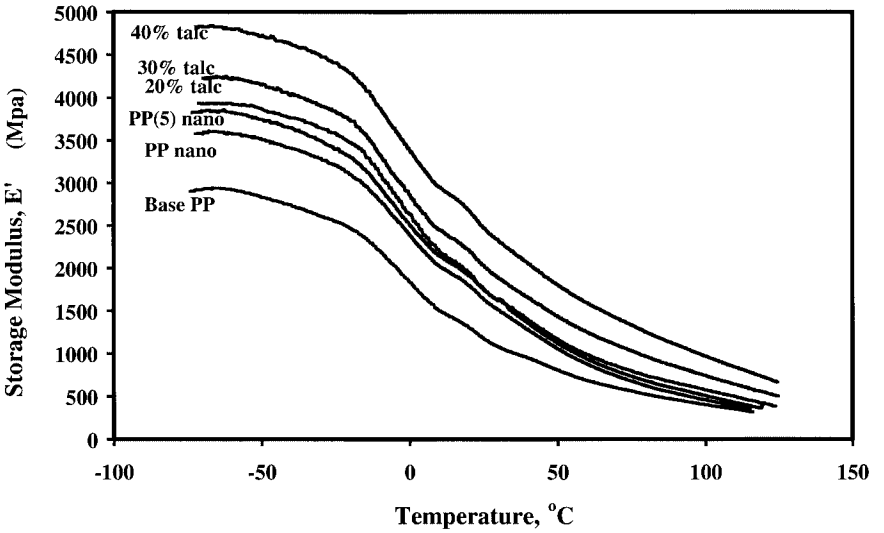

Figure 4 E'' of HCPP and nanocomposite blends with PP.

around 0°C for PP and is unaffected by the presence of the clay. When a fully exfoliated nanocomposite is produced, the particles do not behave like typical filler particles. They have the ability not only to impart a higher heat deflection temperature but also to increase the measured T_g. Figure 6 summarizes DMTA data for PA-6, M2350, and M1030 nanocomposites. Both TEM micrographs and wide-angle X-ray scattering studies have indicated complete exfoliation of the nanocomposite particles. The increase (10–15°C) in the maximum of log $E''(T_g)$ in the nanocomposites (where E'' is the dynamic mechanical loss modulus) over that of regular PA-6 is accompanied by a significant increase in stiffness (log E', where E' is the dynamic mechanical storage modulus) that is persistent even to relatively high temperatures. Moreover, the maxima of the secondary or β relaxations, which are associated with very small-scale molecular motions, are shifted to higher temperatures in the nanocomposites, and this confirms the molecular scale origin of the effects of the nanoparticulate.

This is consistent with the morphological data discussed previously and also contrasts with the reported behavior of PA-6 nanocomposites, which exhibited an upward shift of approximately 10–15°C in T_g.[1] For PA-6, the latter behavior has been attributed in part to the complete exfoliation of the clay. The peak in Figure 5 at approximately 45°C becomes larger as the clay (concentrate) content increases and is associated with the increased MA–PP content that is present in the concentrate.

A summary of the response of the storage modulus, which correlates directly with the stiffness or flexural modulus, indicates that the PP nanocomposite is very

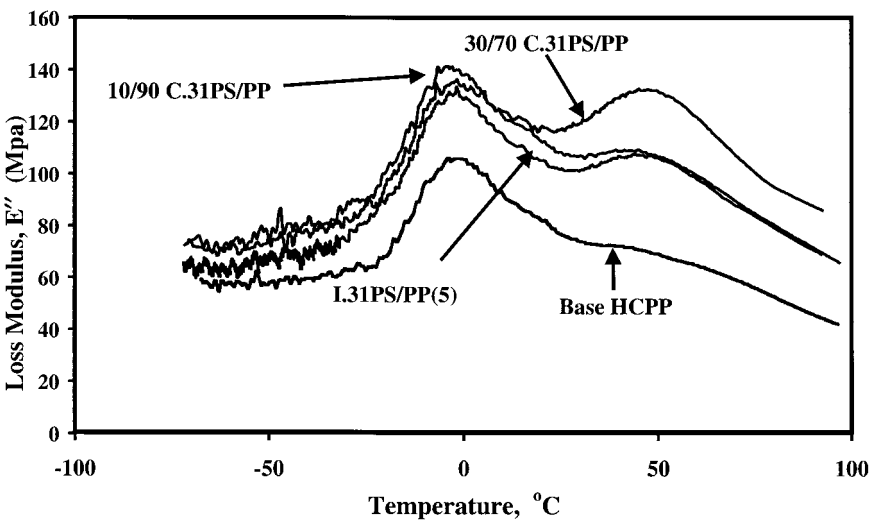

Figure 5 E' of TFPP and PP nanocomposites (I.31PS/PP).

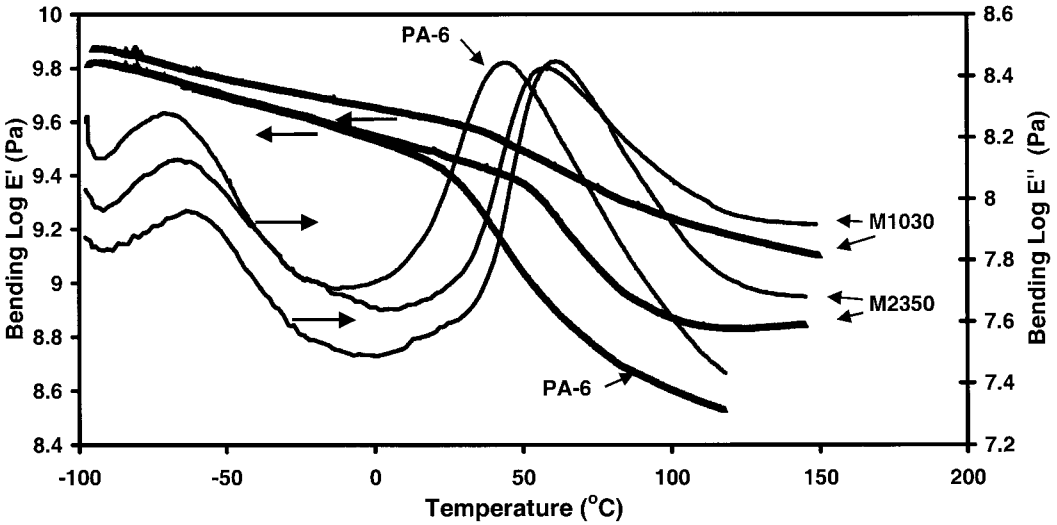

Figure 6 Log E' and log E'', measured at 1 Hz by dynamic mechanical analysis, of PA-6 and PA-6 nanocomposites containing 2 (M2350) and 4 wt % (M1030), respectively, of a nanoparticulate.

similar to 20% TFPP. As the temperature increases up to 75°C, the clay has little influence in preserving the stiffness of PP. Once again, this behavior contrasts markedly with that observed in the PA-6 nanocomposites shown in Figure 6. The extended processing cycle appears to have little effect on the response to DMTA, and this indicates that the increased mixing time has little influence on dispersion and that the nanocomposite is thermally stable.

SG

The measured values of SG are shown in Figure 7. The 20, 30, and 40 wt % TFPPs have values of 1.06, 1.15, and 1.24 g cm^{-3}, respectively, all of which are in good agreement with the specification values. This is also true for PP, which has a measured SG of 0.91 g cm^{-3} and a specification value of 0.89–0.93 g cm^{-3}. The nanocomposite has a measured increase of only 0.02 g cm^{-3}, which corresponds to weight savings of 12.3 and 25% for the 20 and 40 wt % TFPPs, respectively. The blend of 40 wt % TFPP with the PP nanocomposite (see Table IV) has a measured SG of 1.08 g cm^{-3}. The latter result signifies weight savings of 6 and 13% over the 30 and 40 wt % TFPPs, respectively; as discussed later, this provides a mechanical performance similar to that of 30 wt % TFPP.

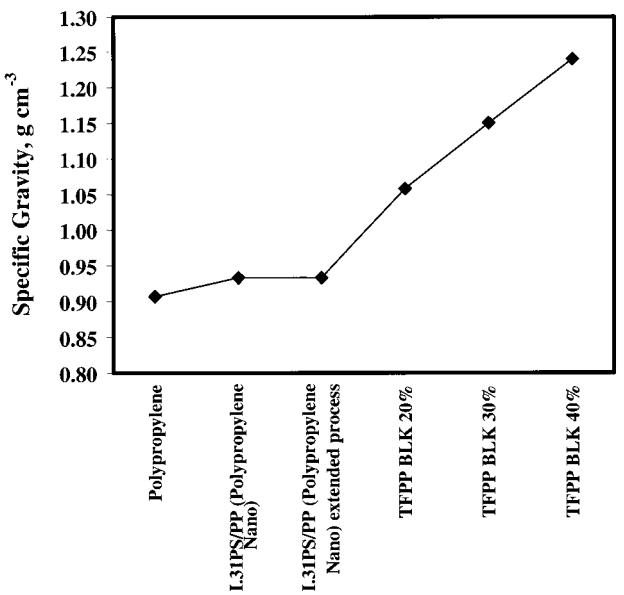

Figure 7 SG of PP nanocomposites and TFPPs.

Mechanical properties

The tensile and flexural properties are summarized in Table IV. A selection of the tabulated properties, derived only from the data obtained from the DSM minimolder, are also shown schematically in Figure 8. All the samples had an extension at break greater than 50%. The data in Table IV include measurements under different test conditions and from different sample preparations for comparison.

The test specimens made with the DSM mini-injection molder were not intended to provide definitive mechanical property data; however, we have the advantage of comparing our results with data obtained from small, 2-mm-thick ISO bars that were cut from plaques molded for a rigorous study[15] of talc-filled materials. The data in Table IV indicate that the agreement in the measurements of the tensile moduli for the TFPPs with these different fabrication and test protocols is very good. Therefore, we believe that the data comparison within the set including the nanocomposite is very good and that the data are in close agreement with more conventional sample preparation procedures.

TABLE IV
Mechanical Properties of PP Materials and PP Nanocomposites at 25°C

Sample	Tensile maximum load (N)	Tensile maximum stress (MPa)	Tensile modulus (GPa)	Flexural maximum load (N)	Flexural maximum stress (MPa)	Flexural modulus (GPa)
PP	290	38.1	1.97	84	67.9	1.89
I.31PS/PP	296	38.7	2.38	83	66.3	2.13
I.31PS/PP (extended process)	308	40.2	2.40	—	—	—
40% TFPP (50%), C.31PS (5%), I.31PS/PP (45%)	282	37.6	3.11	81	64.3	2.75
20% TFPP	269 (294)	35.2 (30.6)	2.34 (2.38)	78	61.0 [42.3]	2.27 [2.99]
30% TFPP	270 (307)	35.3 (32)	3.13 (3.15)	—	—	—
40% TFPP	259 (302)	33.9 (31.7)	3.65 (3.66)	73	57.9 [44.1]	3.29 [4.67]
C.31PS (10%)/PP (90%)	304	40.7	2.43	—	—	—
C.31PS (20%)/PP (80%)	305	41	2.71	—	—	—
C.31PS (30%)/PP (70%)	302	40.2	2.92	—	—	—

Parentheses indicate a strain rate of 0.1 cm/cm/min and ISO bars cut from injection-molded plaques in the flow direction measured at room temperature. Brackets indicate a flexural ramp rate of 0.05 in./min, a span of 2.0 in; LVDT, displacement (0–0.015 in.) was used, and the sample was cut from injection molded plaques in the flow direction measured at room temperature.[15]

Reports in the literature[6] have indicated that the flexural modulus of a PP nanocomposite increased to 2.1 GPa from 1.5 GPa of unmodified PP.

The flexural data in Table IV indicate a modest improvement, particularly with respect to the modulus. We suspect that the value of 1.89 GPa that we have recorded for the flexural modulus of HCPP may be unusually high. The values recorded for the maximum tensile stress or tensile strength are in reasonable agreement with literature values.[15] The nanocomposite materials retain their tensile strength or have a slightly improved tensile strength in comparison with the talc-filled materials.

Some mechanical testing at elevated temperature was also performed. The ambient flexural modulus of the PP nanocomposite was measured to be 2.13 GPa. The modulus was found to decrease to 1.3 GPa at approximately 49°C (120°F) and reflects observations noted during the DMTA studies. The latter contrasts with a value of 1.2 GPa measured at a 2.5-mm deflection for a 20 wt % talc-filled sample. The tensile strengths at yield at the ambient temperature and 49°C for the nanocomposite were recorded to be 38.9 and 27.4 MPa, respectively. We report a value of 25.7 MPa at 49°C for 20 wt % TFPP, once again indicating the slightly better performance of the PP nanocomposite at an elevated temperature.

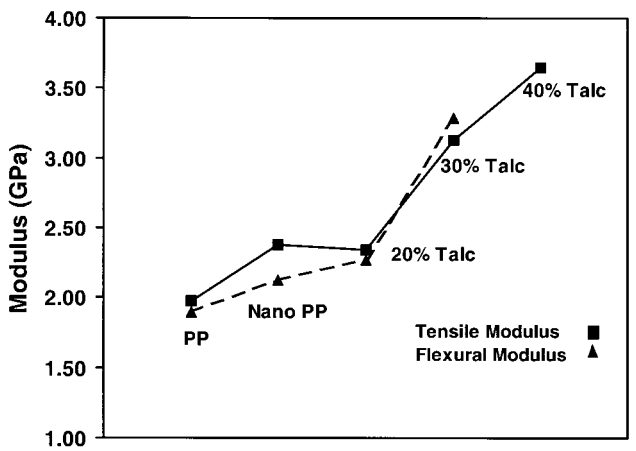

Figure 8 Tensile and flexural moduli of PP and PP compositions.

Formulations derived from the concentrate (10, 20, and 30 wt %) and HCPP, without added compatibilizer, were found to increase the tensile modulus at each increment. The latter formulations correspond to clay levels of approximately 5, 10, and 15 wt %, respectively, and this is a considerably greater scaling of the filler content than that produced in the increase in the tensile modulus. A formulation based on the concentrate, PP nanocomposite, and 40 wt % TFPP indicated a tensile modulus comparable to that of 30 wt % TFPP. The latter result suggests a number of options in blending talc and nanocomposite fillers to tailor a balance of stiffness and density.

CONCLUSIONS

The PP nanocomposites prepared in this work have been shown to offer improved stiffness and tensile modulus without the penalty of increased density that usually accompanies a mineral-filled polymer. However, we have found distinct morphological differences between the PP nanocomposite examined here and typical polyamide nanocomposites in which complete exfoliation can dramatically improve some mechanical properties. XRD and microscopy have shown the composite to possess well-dispersed clay particles intercalated by the polymer. Complete exfoliation, or dispersion of the silicate layers of the clay into individual platelets, is largely absent. This has also been

confirmed by permeability measurements in toluene demonstrating no improvement in the permeability between the nanocomposite and the base PP. In the context of additional studies[16] on polyamide-based nanocomposites, we propose that permeability measurements may be useful in characterizing the state of exfoliation of the nanocomposite filler in a polymer.

The melting behavior and T_g are unaffected with respect to those of the base PP and TFPP. This contrasts markedly with the known behavior observed in polyamide nanocomposites, for which an increase of approximately 10°C in T_g has been measured, and again signifies important differences in the morphologies of these nanocomposite materials. DMTA indicates that the stiffness of the PP nanocomposite, from 0 to 70°C, is comparable to that of 20 wt % TFPP.

The mechanical performance of the PP nanocomposite shows a significant improvement over the base material, and the improvements are comparable to those reported in the literature. The benefits are not as great as those reported for PA-6-based nanocomposites, and the reason for this probably resides with the incomplete exfoliation of the treated clay. The mechanical properties, such as the flexural modulus and tensile strength of the PP nanocomposite, are at least comparable to those of 20 wt % TFPP. SG measurements have shown that the latter can be achieved with a 12% mass saving. A melt-compounded hybrid blend of the nanocomposite and 40 wt % TFPP has been shown to have mechanical properties representative of a 30 wt % talc-filled material and to be accompanied by a 6 wt % weight reduction.

The contributions and provision of experimental materials by Gerry Qian and Ron Gartner of Nanocor, Inc., and by Kurt Mittlefehldt and Sue Beabout of Delphi Automotive Systems are gratefully acknowledged. Analytical data were also provided by Mike Balogh of General Motors Research and Development and Planning and by Brian Gillispie, Scharron Rambus, and John Krohn of Delphi Research Labs.

References

1. Kojima, Y.; Usuki, A.; Kawasumi, M.; Okada, A.; Fukushima, Y.; Kurauchi, T.; Kamigaito, O. J Mater Res 1992, 8, 1185.
2. Usuki, M. K.; Kato, A.; Okada, A.; Kurauchi, T. J Appl Polym Sci 1997, 63, 137.
3. Heinemann, J.; Reichert, P.; Thomann, R.; Mulhaupt, R. Macromol Rapid Commun 1999, 20, 423.
4. Hasegawa, N.; Kawasumi, M.; Kato, M.; Usuki, A.; Okada, A. J Appl Polym Sci 1998, 67, 87.
5. Kato, M.; Usuki, A.; Okada, A. J Appl Polym Sci 1997, 66, 1781.
6. Kurokawa, Y.; Yasuda, H.; Kashiwagi, M.; Oyo, A. J Mater Sci Lett 1997, 16, 1670.
7. Kawasumi, M.; Hasegawa, N.; Kato, M.; Usuki, A.; Okada, A. Macromolecules 1997, 30, 6333.
8. Hasegawa, N.; Okamoto, H.; Kato, M.; Usuki, A. J Appl Polym Sci 2000, 78, 1918.
9. Hambir, S.; Bulakh, N.; Jog, J. P. Polym Eng Sci 2002, 42, 1800.
10. Svoboda, P.; Zeng, C. C.; Wang, H.; Lee, L. J.; Tomasko, D. L. J Appl Polym Sci 2002, 85, 1562.
11. Krishnamoorti, R.; Vaia, R. A.; Giannelis, E. P. Chem Mater 1996, 8, 1728.
12. Mouzakis, J.; Karger-Kocsis, J. J Appl Polym Sci 1998, 68, 561.
13. Philips, R. A.; Wolkowicz, M. D. In Polypropylene Handbook; Moore, E. P., Ed.; Hanser/Gardner: Cincinnati, 1996; p 113.
14. Subramanian, P. M.; Plotzker, I. G. In Polymer Blends: Formulation and Performance; Paul, D. R.; Bucknall, C. B., Eds.; Wiley: New York, 2000.
15. Novak, G. E. Delphi Research Labs., 2001, unpublished data.
16. Ellis, T. S. Polymer, in press, 2003.